

Optics Letters

Fabrication of an anti-reflective microstructure on sapphire by femtosecond laser direct writing

QIAN-KUN LI,¹ JIA-JI CAO,² YAN-HAO YU,¹ LEI WANG,¹ YUN-LU SUN,¹ QI-DAI CHEN,^{1,*}
AND HONG-BO SUN^{1,2}

¹State Key Laboratory on Integrated Optoelectronics, College of Electronic Science and Engineering, Jilin University, Changchun 130012, China

²College of Physics, Jilin University, Changchun 130012, China

*Corresponding author: chenqd@jlu.edu.cn

Received 1 December 2016; revised 22 December 2016; accepted 29 December 2016; posted 3 January 2017 (Doc. ID 281936);
published 27 January 2017

Herein, we report a facile approach for the maskless production of subwavelength-structured antireflective surfaces on sapphire with high and broadband transmittance in the mid-IR: femtosecond laser direct writing assist with wet etching. With this method, inverted pyramid and cone arrays with a pitch of about 2 μm and a total height of near 900 nm on the sapphire were produced. The resulting subwavelength structures greatly suppress specular reflection at normal incidence. The transmission measurements between 3 and 5 μm are in agreement with the simulations performed using VirtualLab, and the transmittance reached a maximum value of 92.5% at 4 μm . The sapphire with subwavelength structures also exhibits angle-independent transmittance characteristics up to a high $\theta = 60^\circ$. Therefore, these subwavelength structures on sapphire are of great technological importance in mid-IR optics, especially for the harsh-condition-applicable windows of military mid-IR devices. © 2017 Optical Society of America

OCIS codes: (310.6628) Subwavelength structures, nanostructures; (350.3390) Laser materials processing; (220.4000) Microstructure fabrication.

<https://doi.org/10.1364/OL.42.000543>

Today, surface antireflection techniques are indispensable for improving the performance of many optical and optoelectronic devices, such as solar cells, flat panel displays, and optical detectors [1–4]. Usually, surface coatings based on single or multi-layer interference structures with alternating high and low refractive indices are employed for the antireflection [5,6]. However, the problems of films shedding or cracking due to thermal expansion or low-temperature shrinkage and mechanical scratching are often encountered [6]. Inspired by moth eyes, an alternative to surface coatings are subwavelength-structured antireflective surfaces that provide a graded transition between the refractive indices of the two interfacing media [7–13]. The subwavelength structures (SWSs) can overcome the above problems of surface coatings because they have the same material constitutions as the substrate. Previous studies showed that the

reflectivity can be significantly suppressed for a wide spectral bandwidth and over a large angle of incidence [14,15]. Nano-imprint lithography or dry etching methods are usually applied to realize masters for SWSs, in which shadow or imprinting masks with resolutions on the subwavelength scale are required [16–22]. The masks can be obtained by self-assembly, e-beam or laser interference lithography, or from natural materials [14–18]. However, the practical applications are highly restricted by the high cost of the masks or the complexity of the procedures. Femtosecond laser direct writing (FsLDW) is a maskless, facile, and rapid writing method that can realize arbitrary, designable, and complicated structures and therefore is a promising solution to the issues described above [23–27].

Sapphire is one of the most widely used optical window materials because of its high hardness, thermal and chemical stabilities, and high optical transparency from the mid-IR to the UV region. However, the light transmittance efficiency of a sapphire surface is not sufficiently high for many applications due to the relatively high reflectivity at the air/sapphire interface caused by the large refractive index of sapphire. In this work, SWSs on sapphire fabricated by FsLDW assisted by subsequent wet etching for mid-IR antireflection have been demonstrated. The SWSs introduce a gradient in the refractive index between air and the sapphire substrate, which dramatically suppresses the surface reflective loss from the mid-IR regions with an incidence angle up to 60° . Additionally, such surfaces exhibit higher mechanical stability and better durability than coatings because no foreign materials are involved.

In our experiments, a high numerical aperture ($\text{NA} = 0.85$, $80\times$) objective lens was used to tightly focus femtosecond laser pulses to process samples of a $430\text{-}\mu\text{m}$ thickness c-plane sapphire (Hefei Kejing Materials Technology Co., Ltd.). Here, laser pulses are generated from a Ti:Sapphire fs laser amplifier (Spectra-Physics, 120 fs pulse duration, 800 nm wavelength, and 2.5 kHz repetition rate). A BBO crystal was used to get 400-nm laser light for fabrication. The pulse energy was measured in front of the objective lens. To achieve three-dimensional (3D) microstructures, the complicated 3D geometry of microstructures was numerically designed in C# and then converted to computer processing data for 3D scanning.

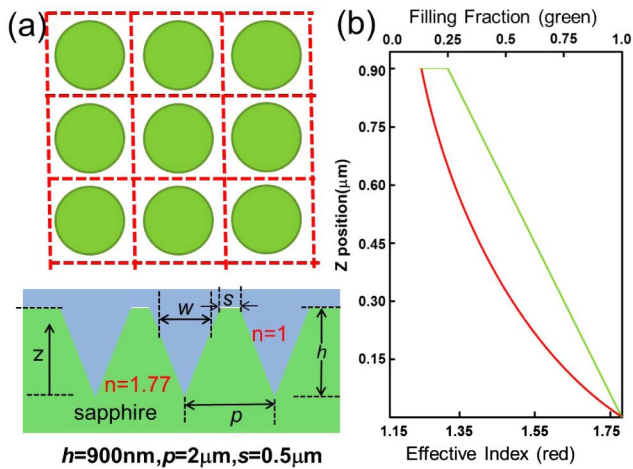


Fig. 1. (a) Front and cross-sectional views of the designed SWSs. They are made by laser ablation of the inverted cone in the substrate. The filling fraction increases toward the substrate, gradually increasing the index. The specific design parameters are: $h = 900$ nm, $p = 2$ μm , and $s = 0.5$ μm . The width w is a function of the z coordinate. (b) Fill fraction $f(z)$ (green) and effective index $n_{\text{eff}}(z)$ (red) for the design geometry of the sapphire with $n_s = 1.77$. The effective index is calculated using the effective medium theory.

The beam's vertical movements were realized by a piezo stage with 1-nm precision (PI P-622 ZCD). Simultaneously, a two-galvano-mirror set was used to control the sample's horizontal scanning. The scanning electron microscopy (SEM) characterization was carried out using a field emission scanning electron microscope (JSM-7500F; JEOL, JEOL Ltd., Tokyo, Japan). Here, the optical performances of the SWSs on sapphire were evaluated by a Fourier transform infrared spectrometer (Nicolet 6700).

The concept of the SWSs is depicted in Fig. 1. The structure has an array of units with an inverted cone surface, and its pitch should be shorter than half the wavelength of the incident light in order to function as an antireflection structure. As in all SWSs, the goal is to achieve a gradient in the refractive index through an increase in the area fill fraction of the material as radiation propagates in the $-z$ direction. For surface antireflective properties, the gradual change of the refractive index from air to bulk is crucial. With an appropriately designed gradient, reflections can be minimized over a broad range of spectra. This transition of the refractive index is realized by increasing the material density from air to the sapphire inverted cone array, finally merging them into the bulk sapphire. For the planar sapphire substrate, the refractive index abruptly changes from 1.0 to 1.77 (at 4 μm) across the air/sapphire interface, resulting in high reflection. For the sapphire substrate with inverted cone arrays, the effective index is almost continuously changed from 1 to 1.77, leading to minimal reflection. The fill fraction for our nominal design, defined as $f(z) = w(z)/p$, is shown in Fig. 1(b). The approximate reflection properties of a material can be calculated using the effective medium theory (EMT), which gives a conversion from $f(z)$ to an effective index n_{eff} , which is also shown in Fig. 1(b) [28].

Laser processing and wet etching parameters all have significant influence on the geometry quality and surface quality of processed sapphire have been described in detail in our previous

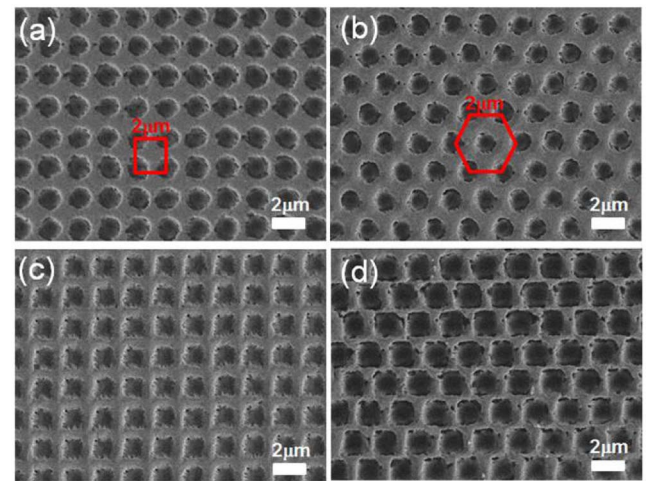


Fig. 2. SEM image of different types of subwavelength gratings fabricated on sapphire: (a) inverted cone array square arrangement, (b) inverted cone array hexagonal arrangement, (c) inverted pyramid array square arrangement, and (d) inverted pyramid array hexagonal arrangement.

work [29]. Shown in Fig. 2 are the SEM images for the fabricated SWSs in sapphire with different arrangements prepared by FsLDW and subsequent wet etching use our optimized best laser processing parameters. The concave structures have a huge advantage in that the removal of material by laser ablation is one of the seven points compared with convex structures, so the laser processing time has dramatically reduced. Additionally, FsLDW can "write" out arbitrary and designable structures that self-assembly-assisted dry etching and lithography technology could not realize [6]. The processed data are the inverted cone and pyramid array, but debris and wet etching have certain influences on the shapes of the structures. So, edges and corners become not obvious, and the final processed structure looks like a paraboloidal profile. Square and hexagonal arrangement SWSs in sapphire have different fill fractions, so the effective index at the interface is slightly different. Under the circumstances, the transmittances of SWSs with different arrangements also have a slight difference, as demonstrated in the experiment shown in Fig. 5.

The planar periodicity of SWSs is important to guarantee homogeneous transmission at different optical windows, but it is not a prerequisite for antireflection. The structure depth and shape determine the transmission rate of an SWS [30]. The approximate theoretical minimum depth of the structured layer reaching 100% transmittance is determined by the following formula [30]:

$$d_{\min} = \frac{\lambda}{4\sqrt{n_1 n_2}}, \quad (1)$$

where λ is the propagating wavelength, and n_1 and n_2 are the refractive indexes of air and the optical substrate, respectively. Given $n_2 = 1.77$ for sapphire at a typical infrared wavelength of $\lambda = 5$ μm , we have $d_{\min} = 0.71$ μm . The actual depth of the SWSs on the surface of the sapphire is more than d_{\min} (approximately 900 nm), which was demonstrated by atomic force microscope (AFM), as shown in Fig. 3. Figure 3(b) shows the cross section at the central line of the SWSs shown in

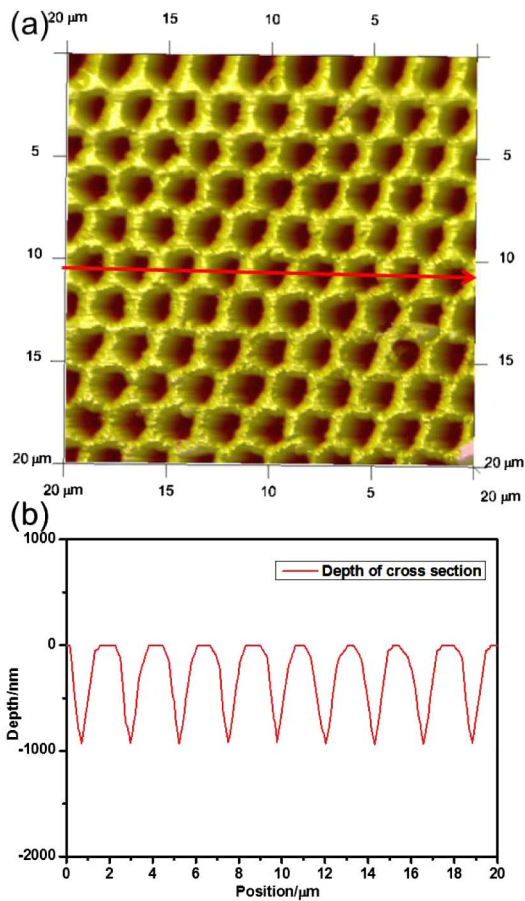


Fig. 3. (a) AFM characterization exhibiting 3D morphology of SWSs. (b) The depth of the subwavelength grating obtained by the cross section of the AFM image.

Fig. 3(a) and shows that the depth controllability of the SWSs is excellent.

The surface roughness is also an important parameter influencing optical performance. Figures 4(a) and 4(b) show SEM images of fabricated SWSs on sapphire with and without etching. Obviously, the surface roughness of SWSs on sapphire after wet etching for 6 min in a mixture of sulfuric acid and phosphoric acid (3:1) at 300°C decreases conspicuously compared with SWSs without etching. The SWSs' surfaces have properties similar to the nipple arrays on the cornea of a moth [7] and dramatically suppress the reflection loss and increase the transmission of light. Figure 4(c) shows the measured transmittance for the SWSs with and without etching in sapphire in the waveband of 3 to 5 μm . It is obvious that an increase of the total transmission after etching was observed over a spectral range from 3 to 5 μm , and at $\lambda = 4 \mu\text{m}$, the transmittance reached a maximum value of 92.5%. Before etching, the debris on the surface and periodic nanostructure induced by laser processing caused diffuse reflection, resulting in the deterioration of the optical performance. A plane sample was measured in each case as a reference.

The optical properties of the SWSs in sapphire were characterized with Fourier-transform infrared spectrometry. Figure 5(a) shows the theoretical simulations (VirtualLab Fusion: grating toolbox) of the transmittance of inverted cone and pyramid

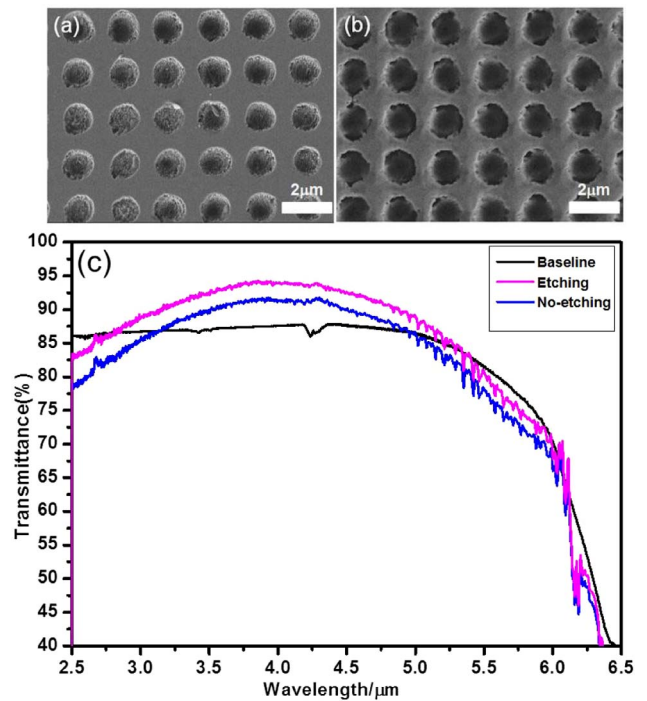


Fig. 4. (a) SEM image of SWSs on sapphire without wet etching. (b) SEM image of SWSs on sapphire after etching. (c) Measured transmittance of fabricated SWSs on sapphire with wet etching and without etching.

arrays. The SWS surfaces exhibit transmittance of about 95% over a spectral range from 3 to 5 μm under the condition of the parameters in Fig. 1. Figure 5(b) shows the measured specular transmittances of different arrangements of SWSs. The transmittance of the SWS surfaces is over 90% from 3 to 5 μm , and different arrangements and profiles of structures have little difference of transmittance. This is because that when the grating period is smaller than or equal to half the working wavelength and the height is fixed, the surface profile has little impact on the transmittance [6]. Theoretically, structuring both surfaces of the sapphire can further increase the transmittance. A higher transmittance could be obtained using a large-scale piezo stage and a high repetition frequency laser in the future. Incident-angle-dependent transmission is another important parameter to investigate. Figure 5(c) shows the sapphire with SWSs exhibits angle independence up to 80° transmittance and reflection characteristics as a function of the incident angle for unpolarized light at a wavelength of 4 μm in the simulations. As shown in Fig. 5(d), the transmittance of the SWSs in the sapphire is over 90% from 3 to 5 μm for the incidence angle of up to 60° in the experiment.

In conclusion, we have demonstrated the first use of laser ablation and the wet etching method to produce mid-IR wave SWSs on hard, difficult-to-machine sapphire. By applying the SWSs to the surface of the sapphire, higher transmittance spectra ($T = 90\%$) were achieved at wavelengths ranging from 3 to 5 μm , exhibiting the less-angle-dependent transmittance property up to a high $\theta = 60^\circ$. The theoretically calculated transmittance results showed a similar tendency to the experimentally measured data. Besides the remarkable optical properties, these structures offer additional advantages compared to thin-film coatings in terms of mechanical stability and durability because

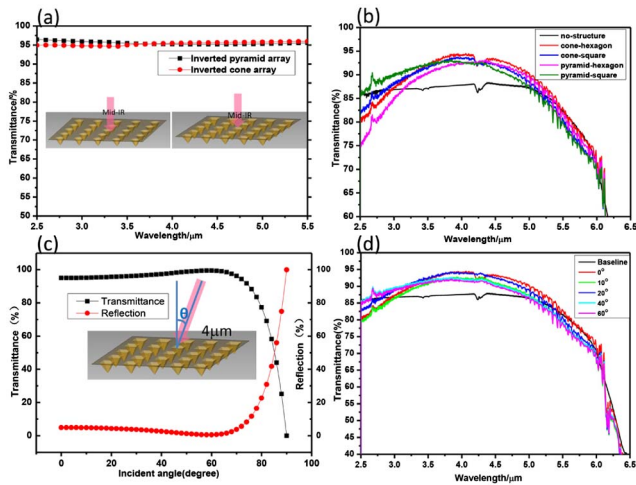


Fig. 5. (a) Theoretical simulations of transmittance of designed SWSs. (b) Measured transmittance of fabricated SWSs. (c) Theoretical simulations of transmittance versus incident angle (incident light wavelength: 4 μm). (d) Measured transmittance versus incident angle.

they are essentially free of mechanical adhesion problems and tensile stress. The method represents an inexpensive, maskless, and very reproducible way to fabricate highly light-transmissive, antireflective optical materials to be used for optical detectors and navigation systems.

Funding. National Natural Science Foundation of China (NSFC) (61137001, 61590930, 61435005, 91423102, 91323301).

REFERENCES

- A. Rahman, A. Ashraf, H. Xin, X. Tong, P. Sutter, M. D. Eisaman, and C. T. Black, *Nat. Commun.* **6**, 5963 (2015).
- Y. F. Huang, S. Chattopadhyay, Y. J. Jen, C. Y. Peng, T. A. Liu, Y. K. Hsu, C. L. Pan, H. C. Lo, C. H. Hsu, Y. H. Chang, C. S. Lee, K. H. Chen, and L. C. Chen, *Nat. Nanotechnol.* **2**, 770 (2007).
- Y. F. Li, J. H. Zhang, S. J. Zhu, H. P. Dong, F. Jia, Z. H. Wang, Z. Q. Sun, L. Zhang, Y. Li, H. B. Li, W. Q. Xu, and B. Yang, *Adv. Mater.* **21**, 4731 (2009).
- C. Lee, S. Y. Bae, S. Mobasser, and H. Manohara, *Nano Lett.* **5**, 2438 (2005).
- M. S. Park, Y. Lee, and J. K. Kim, *Chem. Mater.* **17**, 3944 (2005).
- H. K. Raut, V. A. Ganesh, A. S. Nair, and S. Ramakrishna, *Energy Environ. Sci.* **4**, 3779 (2011).
- P. B. Clapham and M. C. Hutley, *Nature* **244**, 281 (1973).
- P. Vukusic and J. R. Sambles, *Nature* **424**, 852 (2003).
- J. Yang, F. F. Luo, T. S. Kao, X. Li, G. W. Ho, J. Teng, J. H. Teng, X. G. Luo, and M. H. Hong, *Light Sci. Appl.* **3**, e185 (2014).
- P. Spinelli, M. A. Verschuuren, and A. Polman, *Nat. Commun.* **3**, 692 (2012).
- C. F. Guo, T. Y. Sun, F. Cao, Q. Liu, and Z. F. Ren, *Light Sci. Appl.* **3**, e161 (2014).
- T. Lohmüller, M. Helgert, M. Sundermann, R. Brunner, and J. P. Spatz, *Nano Lett.* **8**, 1429 (2008).
- W. L. Min, B. Jiang, and P. Jiang, *Adv. Mater.* **20**, 3914 (2008).
- L. Wang, B. B. Xu, Q. D. Chen, Z. C. Ma, R. Zhang, Q. X. Liu, and H. B. Sun, *Opt. Lett.* **36**, 3305 (2011).
- X. Chen, Z. C. Fan, Y. Xu, G. F. Song, and L. H. Chen, *Microelectron. Eng.* **88**, 2889 (2011).
- G. Zhang, J. Zhang, G. Xie, Z. Liu, and H. Shao, *Small* **2**, 1440 (2006).
- C. H. Sun, W. L. Min, N. C. Linn, P. Jiang, and B. Jiang, *Appl. Phys. Lett.* **91**, 231105 (2007).
- Y. Zhao, J. Wang, and G. Mao, *Opt. Lett.* **30**, 1885 (2005).
- S. Wang, X. Z. Yu, and H. T. Fan, *Appl. Phys. Lett.* **91**, 061105 (2007).
- J. W. Leem and J. S. Yu, *Opt. Express* **20**, 26160 (2012).
- X. Ye, J. Huang, F. Geng, L. Sun, H. Liu, X. Jiang, and W. Zheng, *IEEE Photon. J.* **8**, 1 (2016).
- Y. H. Ko and J. S. Yu, *Opt. Express* **19**, 15574 (2011).
- H. Imamoto, S. Kanehira, X. Wang, K. Kametani, M. Sakakura, Y. Shimotsuma, K. Miura, and K. Hirao, *Opt. Lett.* **36**, 1176 (2011).
- G. Q. Du, Q. Yang, F. Chen, H. W. Liu, Z. F. Deng, H. Bian, S. G. He, J. H. Si, X. W. Meng, and X. Hou, *Opt. Lett.* **37**, 4404 (2012).
- K. Sugioka and Y. Cheng, *Light Sci. Appl.* **3**, e149 (2014).
- S. Juodkazis, K. Nishimura, H. Misawa, T. Ebisui, R. Waki, S. Matsuo, and T. Okada, *Adv. Mater.* **18**, 1361 (2006).
- R. Kammel, R. Ackermann, J. Thomas, J. Gotte, S. Skupin, A. Tunnermann, and S. Nolte, *Light Sci. Appl.* **3**, e169 (2014).
- R. Bräuer and O. Bryngdahl, *Appl. Opt.* **33**, 7875 (1994).
- Q. K. Li, Y. H. Yu, L. Wang, X. W. Cao, X. Q. Liu, Y. L. Sun, Q. D. Chen, and H. B. Sun, *IEEE Photon. Technol. Lett.* **28**, 1290 (2016).
- D. H. Raguin and G. M. Morris, *Appl. Opt.* **32**, 1154 (1993).